PAPER

Check for updates

Two d^{10} luminescent metal–organic frameworks as dual functional luminescent sensors for (Fe^{3+},Cu^{2+}) and 2,4,6-trinitrophenol (TNP) with high selectivity and sensitivity†

Xiaojing Zhou, [iD] *[a] Xiaolei Guo,[b] Lili Liu,[a] Haidong Zhai,[a] Qingguo Meng, [iD] [a] Zhan Shi [iD] [b] and Xishi Tai*[a]

Two luminescent 3D supramolecular structures [Cd$_3$(L)$_2$(2,2-bipy)$_2$](DMF)$_3$(CH$_3$CH$_2$OH)$_2$(H$_2$O) (**1**) and [Zn$_3$(L)$_2$(2,2-bipy)$_2$(DMF)$_2$](DMF)$_2$(CH$_3$CH$_2$OH)$_2$(H$_2$O) (**2**) (H$_3$L = 4,4′,4″-nitrilotribenzoic acid) have been successfully synthesized under solvothermal conditions using Cd(NO$_3$)$_2$·4H$_2$O or Zn(NO$_3$)$_2$·6H$_2$O as the metal sources, and 4,4′,4″–nitrilotribenzoic acid (H$_3$L), 2,2-bipy as the ligands in DMF solvent. Compound **1** displays a bi-nodal (2,3,6)-coordinated net with {8^3}$_2${8^6·12^6·16^3}{8}$_6$ topology, compound **2** can be described as a (3,6)-connected 2-nodal net with kgd topology. The phase purity of compound **1** and **2** is characterized by X-ray powder diffraction (XRPD), thermogravimetric analysis (TGA) and Fourier transform infrared (FT-IR) spectroscopy. Compound **1** and **2** can serve as effective luminescent sensors for Fe^{3+}, Cu^{2+} and TNP *via* luminescent quenching.

Introduction

The detection of hazardous explosives and heavy metal ions is of current interest for environmental conservation and national security.[1–4] Nitro aromatics such as nitrobenzene (NB), 1,3-dinitrobenzene (1,3-DNT), 2,4,6-trinitrotoluene (TNT) and 2,4,6-trinitrophenol (TNP), are ingredients of industrial explosives which are found in many unexploded land mines worldwide.[2,3,5–10] Among these nitro explosives, TNP shows more explosive power compared to TNT. TNP is released into the environment during its commercial production and use, leading to the contamination of soil and aquatic systems. Moreover, picramic acid (2-amino-4,6-dinitrophenol), which is the byproduct of metabolism, has ten times more mutagenic activity than TNP.[11–14] Thus, it is very important for the selective and sensitive detection of TNP present in soil and ground water for security screening, homeland security and environmental monitoring.

On the other hand, Fe^{3+} and Cu^{2+} ions are not only the most important elements in environmental systems, but also play important roles in biological processes. In particular, Fe^{3+} ions are of great importance in oxygen uptake and transportation, oxygen metabolism and electron transfer. However, accumulation of Fe^{3+} ions in the human body would damage biomolecules by generating reactive oxygen species (ROS). Meanwhile, iron deficiency could result in diseases such as anemia and insomnia.[15–18] Similarly, exposure to excess Cu^{2+} ions, which may have resulted from environmental contamination and occupational hazards, could lead to oxidative damage. Excess Cu^{2+} uptake can result in copper metabolism disorders in the brain and give rise to diseases such as Alzheimer's disease.[19–22] Hence, selective detection or sensing of Fe^{3+} and Cu^{2+} seems to be very important for human health.

Various traditional methods have been used for monitoring explosives and metal ions including gas chromatography, liquid chromatograph/mass spectrometer, gel chromatography, inductively coupled plasma, atomic absorption spectrophotometry, electrochemical methods, *etc.*[23–27] nevertheless, these detection techniques are limited by their inconvenience of carrying, time-consuming and the like. Compared to the traditional methods, fluorescence detection has obvious advantages and gains more attention owing to its high sensibility, simplicity, short response time, and its ability to be employed both in solution and solid phase. In fact, the materials are usually used for fluorescence detection are still defective in the respects of stability, toxicity, sensitivity, and biodegradability, thus it is a challenging task to synthesize novel materials for fluorescence detection of explosives and metal ions.[28–30]

^{a}School of Chemical & Chemical Engineering and Environmental Engineering, Weifang University, Weifang, 261061, P. R. China. E-mail: zhouxiaojing105@163.com; taixs@wfu.edu.cn

^{b}State Key Laboratory of Inorganic Synthesis & Preparative Chemistry, College of Chemistry, Jilin University, Changchun, 130012, P. R. China

† Electronic supplementary information (ESI) available: Selected bond distances and angles (Table S1 and S2), Stern–Volmer plots of compounds **1** and **2** (Fig. S1–S6), the PXRD data of compounds **1** and **2** (Fig. S7 and S8), IR of compounds **1** and **2** (Fig. S9 and S10), TGA of compound **1** and **2** (Fig. S11), crystallographic data in CIF. CCDC 1580391 (**1**) and 1813685 (**2**). For ESI and crystallographic data in CIF or other electronic format see DOI: 10.1039/c9ra07709j

Metal–organic frameworks are well known for their potential applications in a wide range of areas such as gas storage, separation, catalysis, sensing, drug delivery, food safety and so on. Among these applications, luminescence metal–organic frameworks (LMOFs) provide several advantages over conventional fluorophores.[31–40] Their designable architectures allow improved host–guest interactions and serve as preconcentrators for target analytes. There are many LMOFs had been developed for the detection of explosives and metal ions, for example, Li *et al.* reported the first highly LMOF which is able to detect trace amounts of nitroaromatic explosives (NACs) such as 2,4-dinitrotoluene (DNT) and 2,3-dimethyl-2,3-dinitrobutane (DMNB) in the vapor phase.[41] Subsequently, a series of LMOF based on transition metal ions or lanthanide were documented for sensing and detection of NACs with a fast and highly sensitive response *via* partial luminescence quenching, for example, Shi *et al.* studied the luminescence quenching of $Zn_3(TDPAT)(H_2O)_3 \cdot G$ (G = guest solvent) with the addition of nitrobenzene, and its limit detection is 50 ppm.[42] Bu *et al.* reported a highly sensitive luminescent Cd(II)-based MOF that quenched at 100 ppm of TNP and display a high quenching efficiency of 92.5%.[43] Ghosh's group demonstrated a luminescent 3D MOF $[Cd(NDC)_{0.5}(PCA)] \cdot G_x$ (G = guest molecules, NDC 2,6-napthalenedicarboxylic acid, PCA = 4-pyridinecaboxylic acid) for the highly selective detection of 2,4,6-trinitrophenol (TNP).[44]

However, multifunctional sensors based on LMOFs are relatively rare.[45–47] Therefore the exploitation of dual functional chemosensor for detecting metal ions (*i.e.* Fe^{3+}, Cu^{2+}) that are necessary for the human body and nitroaromatic compounds that harm personal and environmental safety is of great significance.

In this article, we are presenting two 3D supermolecular MOF structures $[Cd_3(L)_2(2,2\text{-bipy})_2(DMF)_3](CH_3CH_2OH)_2(H_2O)$ and $[Zn_3(L)_2(2,2\text{-bipy})_2](DMF)_3(H_2O)$ (**2**), which have been utilized as dual luminescent sensor for the selective detection of metal ions (Fe^{3+}, Cu^{2+}) and TNP, and showed high selectivity and sensitivity through luminescence quenching.

Experimental section

Materials and physical measurements

All reagents and solvents were obtained commercially and used without further purification. Elemental analyses were performed on a PerkinElmer 2400 element analyzer. IR spectra were recorded on a Nicolet Impact 410 FTIR spectrometer using KBr pellet. PXRD data were collected on a Rigaku D/max 2550 X-ray Powder Diffractometer. TGA was measured using thermogravimetric experiments, which were performed with a TGA Q500 V20.10 Build 36; data were collected from room temperature to 800 °C at a heating rate of 10 °C min^{-1} in a flowing N_2 atmosphere.

Synthesis of compound 1

Cd(NO$_3$)$_2 \cdot$4H$_2$O (0.1 mmol, 30.8 mg), **H$_3$L** (0.05 mmol, 18.8 mg), and 2,2′-bipy (0.1 mmol, 15.6 mg) were dissolved in DMF (6 mL).

The resulting reaction mixture was stirred at room temperature for 30 min. Then it was transformed to a 15 mL teflon-lined stainless steel vessel and heated at 100 °C for three days. After this time block brown crystals of **1** were obtained in 57% yield (based on **H$_3$L**), IR (KBr 4000–400 cm^{-1}) 3126 (w), 1669 (s), 1591 (s), 1384 (s), 1172 (m), 1081 (m), 1017 (m), 838 (s), 784 (s), 668 (m), 636 (m), 539 (w), 442 (w). Elemental analysis (%): calcd for: C$_{75}$H$_{75}$Cd$_3$N$_9$O$_{18}$: C 52.10 H 4.34 N 7.29; found: C 52.15 H 4.27 N 7.32.

Synthesis of compound 2

A mixture of Zn(NO$_3$)$_2 \cdot$6H$_2$O (0.1 mmol, 29.1 mg), **H$_3$L** (0.05 mmol, 18.8 mg), 2,2-bipyridine (0.1 mmol, 15.6 mg), DMF (6 mL) were stirred at room temperature for 10 min, then sealed in a 15 mL teflon-lined stainless steel vessel, and heated at 100 °C for three days, after this time columnar colorless crystals of **2** were obtained in 50% yield (based on **H$_3$L**), IR (KBr 4000–400 cm^{-1}) 3469 (w), 3056 (w), 1688 (s), 1585 (s), 1391 (s), 1165 (m), 1101 (m), 849 (w), 778 (s), 668 (m), 520 (s), 436 (w). Elemental analysis (%): calcd for: C$_{74}$H$_{70}$Zn$_3$N$_{10}$O$_{17}$: C 56.69 H 4.47 N 8.94; found: C 56.73 H 4.51 N 8.97.

X-ray crystallography

The data collection and structural analysis were performed on a Rigaku RAXIS-RAPID equipped with a narrow-focus, 5.4 kW sealed tube X-ray source (graphite-monochromated Mo Kα radiation, $\lambda = 0.71073$ Å). The data were collected at a temperature of 20 ± 2 °C. The data processing was accomplished with the PROCESS-AUTO processing program. The structures were solved with the direct methods of SHELXL crystallographic software package and refined on F^2 by full-matrix least square techniques. All non-hydrogen atoms of the two compounds were refined with anisotropic thermal parameters. All hydrogen atoms of the organic molecule were geometrical placed and

Table 1 Crystallographic data and structure refinement summary for compounds **1**, **2**

Compound	**1**	**2**
Molecular formula	C$_{75}$H$_{75}$Cd$_3$N$_9$O$_{18}$	C$_{74}$H$_{70}$Zn$_3$N$_{10}$O$_{17}$
Formula weight	1727.23	1566.23
Crystal system	Monoclinic	Triclinic
Space group	$C2/c$	$P\bar{1}$
a, Å	14.005(3)	13.3539(7)
b, Å	22.005(4)	13.6334(7)
c, Å	23.006(5)	13.6928(7)
V, Å^3	7083(3)	2164.6(2)
Z	4	1
D_{calc}, g cm^{-3}	1.311	1.077
$F(000)$	2776.0	720.0
GoF	1.086	1.085
R_1, wR_2 $[I > 2\sigma(I)]^{a,b}$	$R_1 = 0.0564$	$R_1 = 0.0501$
	w$R_2 = 0.1556$	w$R_2 = 0.1247$
R_1, wR_2 (all data)	$R_1 = 0.039$	$R_1 = 0.0844$
	w$R_2 = 0.0836$	w$R_2 = 0.1141$

^{a} $R_1 = ||F_o| - |F_c||/\Sigma|F_o|$. ^{b} w$R_2 = [\Sigma w(F_o^2 - F_c^2)^2/\Sigma w(F_o^2)^2]^{1/2}$. $w = 1/[\sigma^2(F_o^2) + (ap)^2 + (bp)]$, $p = [\max(F_o^2 \text{ or } 0) + 2(F_c^2)]/3$.

added to the structure factor calculation. CCDC-1580391 (**1**) and CCDC-1813685 (**2**) contain the supplementary crystallographic data for this paper.† Basic information pertaining to crystal parameters and structure refinement is summarized in Table 1. As for the molecular formula of as synthesized compounds **1** and **2**, it is difficult to obtain the exact solvent molecules in the structure, so we further determined it using Platon/Squeeze, TGA, IR and elemental analysis.

Fluorescence experiments

The synthesized sample compound **1** and **2** were immersed in methanol for 24 h, and the extract was decanted. Fresh methanol was subsequently added, and the crystals were allowed to stay for an additional 24 h to remove the methanol solvents. After the removal of methanol by decanting, the sample was activated by drying under a dynamic vacuum at 373 K overnight to obtain the activated samples. The fluorescence experiments of compound **1a** and **2b** were investigated in the solid state and in different solvent emulsions, such as DMF, DMSO, DMA, ethanol, methanol, acetonitrile, water and 1,4-dioxane. The concentration for the suspension was fixed at 3.0 mg compound **1a** or **2b** per 3.0 mL solvents. The luminescence intensities were measured under an excitation of 330, 335 nm for compound **1a** and **2b** respectively. As for the metal ion sensing experiments, $M(NO_3)_x$ ($M = Cd^{2+}$, Co^{2+}, Cu^{2+}, Fe^{3+}, K^+, Na^+, Pb^{2+}, Zn^{2+}) were separately added to DMF suspension of compound **1a** or **2b**. The resulted concentration for the metal ions was 10^{-2} mol L^{-1} and the mixtures were treated by ultra-sonication for 1 h to form a stable suspension. The fluorescence spectra were recorded for the suspensions. For the fluorescence experiments, the solution of $Fe(NO_3)_3$ ($[M] = 10^{-3}$ mol L^{-1}), $Cu(NO_3)_3$ ($[M] = 10^{-3}$ mol L^{-1}), TNP ($[M] = 10^{-3}$ mol L^{-1}) were added gradually into compound **1a** or **2b** DMF suspension, respectively. The fluorescent spectra of the samples were recorded on an Edinburgh Instruments FLS920 spectrofluorimeter equipped with both continuous (450 W) and pulsed xenon lamps.

Results and discussion

Description of crystal structures

Single crystal X-ray crystallographic analysis reveals that compound **1** crystallizes in the monoclinic space group $C2/c$. In this structure, the asymmetric unit of **1** consists of two independent Cd atoms, one L^{3-} ligand, one 2,2-bipy molecule (Fig. 1a). The Cd1 atom is coordinated by four carboxylate O atoms from three L^{3-} ligands, and two N atoms from one 2,2-bipy molecule, adopting an octahedral coordination geometry, Cd1–N and Cd1–O are in the range of 2.314–2.321 Å and 2.186–2.444 Å, respectively, the Cd2 atom is six-coordinated by six carboxylate O atoms from six L^{3-} ligands, has a distorted octahedral coordination geometry (Cd2–O = 2.228–2.298 Å) (Fig. 1b).[48–50] In particular, Cd1, Cd2 atoms are united together through carboxylate groups of L^{3-} ligands to give a central symmetric trinuclear Cd(ɪɪ) cluster (Cd···Cd separation, 3.380–6.760 Å), within the cluster, the Cd2 octahedron is bridged to two symmetry related Cd1 in a corner-sharing manner, each
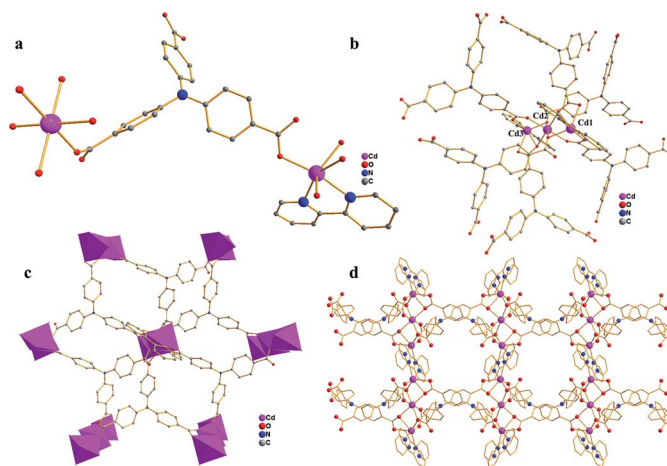

Fig. 1 (a) The asymmetric unit of compound **1**; (b) the coordination sphere of Cd atoms in compound **1**; (c) the 2D layer of compound **1**; (d) the 3D supramolecular structure of compound **1** (purple, Cd; red, O; blue, N; gray, C).
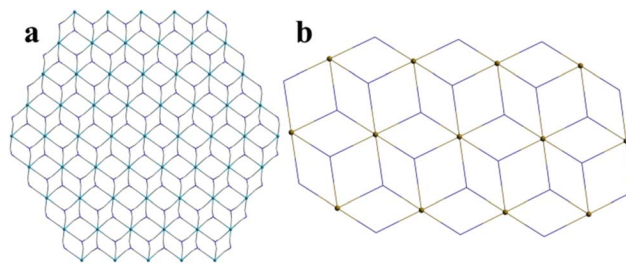

Fig. 2 (a) The topology of compound **1**; (b) the topology of compound **2**.

cluster is linked by six L ligands to form a unique 2D bilayered framework containing quadrangle grids with an approximate dimension of 7.0 Å × 8.8 Å (Fig. 1c). The adjacent bilayers adopt an ABAB mode, with further packing into a 3D supramolecular structure (Fig. 1d), it is noteworthy that π–π interactions between the adjacent 2D layers stabilize the coordination structure. To get deep insight into the structure of compound **1**, topological analysis was carried out. The Cd atom is treated as six-connected nodes, and the L^{3-} ligands are defined as the three-connected nodes, 2,2-bipyridine is considered as two-connected nodes, the layer is simplified as a bi-nodal (2,3,6)-coordinated net with the point symbol $\{8^3\}_2\{8^6 \cdot 12^6 \cdot 16^3\}\{8\}_6$ (Fig. 2a), the calculated solvent accessible volume was 2186.6 Å³ (unit cell volume of 7083.0 Å³), and the porosity was as high as 30.9% by using PLATON.

Single crystal X-ray diffraction analysis reveals that compound **2** crystallizes in the triclinic $P\bar{1}$ space group. As shown in Fig. 3a, the asymmetric unit of **2** contains one Zn(ɪɪ) ion, one L^{3-} unit, one 2,2-bipyridine molecule, and one DMF molecule. Zn1 atom is coordinated by four O atoms from three L^{3-} ligands, two N atoms from one 2,2-bipyridine molecule, showing a distorted octahedral geometry (Zn–O = 1.984–2.381 Å, Zn–N = 2.114–2.188 Å). The Zn2 ion has a six coordinated
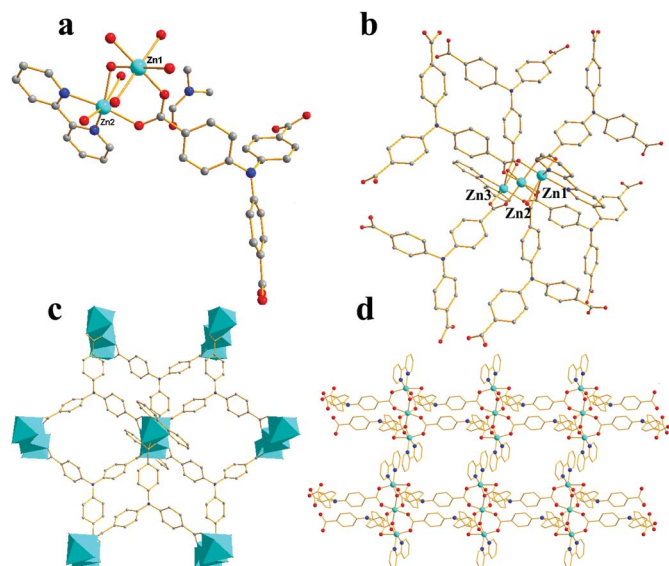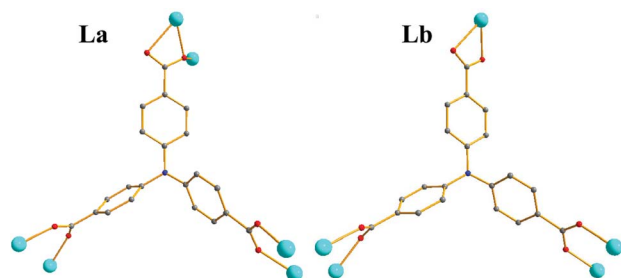
Fig. 3 (a) The asymmetric unit of compound **2**; (b) the coordination sphere of Zn atom in compound **2**; (c) the 2D layer of compound **2**; (d) the 3D supramolecular structure of compound **2** (turquoise, Zn; red, O; blue, N; gray, C).

Scheme 1 Coordination modes of L^{3-}.

octahedral geometry which is defined by six O atoms from four L^{3-} ligands (Zn–O = 2.018–2.160 Å), while Zn3, similar to Zn1, exhibits a distorted octahedral geometry which is formed by four O atoms from three L^{3-} ligands and two N atoms from one 2,2-bipyridine molecule(Zn–O = 1.984–2.381 Å, Zn–N = 2.114–2.188 Å).[49,52] Zn1, Zn2 and Zn3 are associated together by six carboxylate groups of six **H₃L** ligands to form a trinuclear $[Zn_3(CO_2)_6]$ unit, which can be thought of as the secondary building unit (SBU) of the network (Fig. 3b), with distances of Zn1–Zn2 3.4187 Å and Zn1–Zn3 6.836 Å. It is interesting to note that the L^{3-} ligands show two different coordination modes (L_a and L_b), L_a adopts a μ_6-η^1:η^1:η^1:η^2:η^1:η^1 bridging coordination mode to connect six ZnII ions; meanwhile L_b adopts a μ_5-η^1:η^1:η^1:η^1:η^1:η^1 bridging coordination mode to connect six ZnII ions (Scheme 1). The L^{3-} ligands link three adjacent trinuclear Zn(II) cluster to form a 2D sheet with quadrilateral lattices, with a cavity dimension of 8.5 Å × 9.6 Å running along *b* axis (regardless of the van der Waals radii, Fig. 3c), Furthermore, the 2D layers are further linked into a 3D supramolecular architecture through π–π stacking interactions between the 2,2-
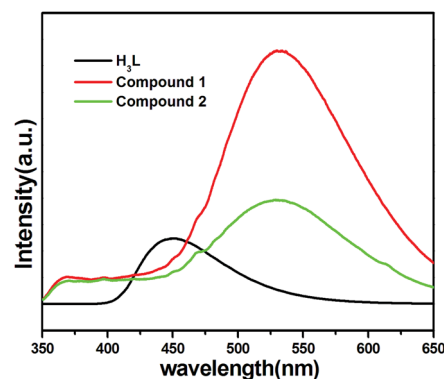

Fig. 4 Solid-state fluorescent spectral of H₃L and compound **1a**, **2b**.

bipy ligands. Without guest molecules, the total accessible volume in compound **2** was estimated to be 36.4% using PLATON software.[12]

To better understand the structure of compound **2**, the topological analysis approach was employed. If defining the L^{3-} ligands as three-connected nodes and the trinuclear Zn(II) cluster as 6-connected nodes, the whole 2D framework can be described as a (3,6)-connected 2-nodal net with a Schläfli symbol of $\{4^3\}_2\{4^6\cdot6^6\cdot8^3\}$, display the kgd topology (Fig. 2b).

Luminescent emission

MOFs have been investigated for fluorescence properties owing to their application in the area of luminescent materials, especially for the compounds with d^{10} metal centers. To further examine the solid state luminescent properties of the d^{10} metal complexes, we measured the solid state fluorescent spectrum of the **H₃L** ligand and the two compounds at room temperature, which are depicted in Fig. 4. The free ligand **H₃L** displays fluorescence with an emissions maximum at 448 nm (λ_{ex} = 330 nm), compound **1** and **2** show fluorescence with emissions maximum at 532 nm and 528 nm respectively (**1**: λ_{ex} = 330 nm, **2**: 335 nm), which has the red shift of 84 or 80 nm, compared with the free **H₃L** ligand. With Zn(II) and Cd(II) as a typical d^{10} configuration, the observed fluorescence emissions should be assigned to ligand-to-metal charge transfer (LMCT), metal-to-ligand charge transfer (MLCT), or intraligand ($\pi^* \rightarrow n/\pi^*$ or $\pi^* \rightarrow \pi$) emission. The luminescent emission of MOFs is influenced by both central metal coordination and the property
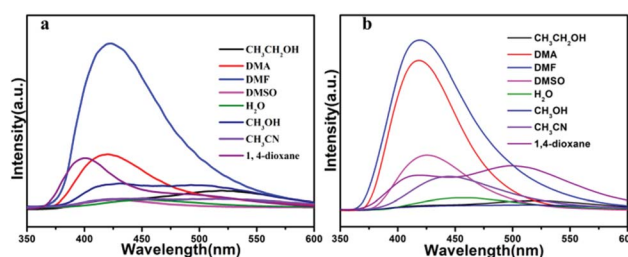

Fig. 5 (a) Fluorescent spectral of compound **1a** in different solvent; (b) fluorescent spectral of compound **2b** in different solvent.

of coordinated ligands, which need to be considered when attempting to assemble new functional luminescent MOFs.[51,52]

The luminescence of the two MOFs encouraged us to examine their potentials for sensing solvent molecules. The fluorescence properties of compound **1a** and **2b** in different solvent emulsions were investigated. The solvents used were DMF, DMSO, DMA, ethanol, methanol, acetonitrile, water and 1,4-dioxane. The fluorescent spectra of the two compounds (3 mg), suspended in the different solvents (3 mL), were measured. As shown in Fig. 5a and b, the emission intensities were dependent on the solvent, meanwhile, there are strong luminescence emissions in DMF solvent compared with other solvents in the two compounds.

Owing to their good fluorescent performance, compound **1a** and **2b** were selected to further study their sensing properties towards various metal ions in DMF solvent. The activated samples **1a** or **2b** (3 mg) were ground into powder, and dispersed in 3 mL of 10^{-2} M suspensions of metal ions: $M(NO_3)_x$ ($M = Cd^{2+}, Co^{2+}, Cu^{2+}, Fe^{3+}, K^+, Na^+, Pb^{2+}, Zn^{2+}$), and then the luminescence experiment was conducted. As depicted in Fig. 6a and b. The solutions that contain different species of metal ions displayed remarkably different luminescent intensities. The results show that the metal ions of Na^+, Zn^{2+} can enhance the fluorescence intensity of activated **1a** with the enhancing percentage of 33%, 35% respectively, we explored the sensitivity of compound **1** for them, after 1000 μL addition of Na^+ or Zn^{2+} (0.01 M) to a 3.0 mL suspension of activated **1a**, it was found that the emission intensity only slightly increased with the enhancing percentage of 4.6% or 4.3%. Meanwhile, part of the metal ions (Cd^{2+}, Na^+ and Zn^{2+}) can enhance the fluorescence intensity of activated **2b** with the enhancing percentage of 13%, 15.5% and 16.3%, respectively, to further explore the enhancing efficiency of Na^+, Zn^{2+} and Cd^{2+} towards activated **2b**, we added 1000 μL Cd^{2+}, Na^+ and Zn^{2+} (0.01 M) to a 3.0 mL suspension of activated compound **2**, it was found that the emission intensity slightly increased with the enhancing percentage of 9.3%, 1.86%, 5.4% for Cd^{2+}, Na^+, Zn^{2+}. The result showed that the quenching effect of these ions towards activated **1a** and **2b** is subtle (Fig. S1 and S2†). As to activated **1a** and **2b**, The other metal ions exhibit different fluorescence quenching efficiency, and the quenching efficiency of compound **1** was calculated to be 16.9, 83.6, 98.9, 99.8, 45.3, 85.8% for $Cd^{2+}, Co^{2+}, Cu^{2+}, Fe^{3+}, K^+$ and Pb^{2+}. For compound **2**, it is estimated that the quenching

efficiency is 17.6, 89.8, 93.2, 100, 99.6% for $Co^{2+}, Cu^{2+}, Fe^{3+}, K^+$ and Pb^{2+}. In particular, Fe^{3+} and Cu^{2+} exhibit an excellent quenching effect with sharply decreased luminescence intensities towards activated compound **1** and **2**, indicating that they can act as promising selective sensor. The possible mechanism of fluorescence quenching is discussed, although framework collapse is always a common way to quench the fluorescence, but as indicated for the PXRD of compound **1a** and **2b** (Fig. S3†), the framework retained its structural integrity after adding into metal ions. Hence, the reason for fluorescence quenching is probably that the interaction between metal ions and the framework changes the electron energy level of ligand, resulting in the inefficient energy transfer between ligand and metal ions.[53,54] In order to further evaluate the fluorescence sensing selectivity performance of the activated samples **1a** and **2b** towards Fe^{3+} and Cu^{2+}, all solid samples (30 mg) were added into 30 mL DMF and got the well-dispersed suspension of probes. Fe^{3+} or Cu^{2+} solution was prepared by dissolving $Fe(NO_3)_3$ or $Cu(NO_3)_2$ in DMF to obtain the desired concentrations (10^{-3} M), the Fe^{3+} or Cu^{2+} ion sensing experiments were performed by adding diverse amounts of above Fe^{3+} or Cu^{2+} ions solution to a quartz cuvette containing 3 mL of DMF suspension of probes and then detected by the PL spectra. The emission intensity was monitored after each addition, the luminescence emission intensity of activated **1a** and **2b** suspended in DMF at 430 nm was leveled off sequentially as a result of gradually increased the volume of Fe^{3+} solution. As shown in Fig. 7a, for the Fe^{3+} towards compound **1**, when the volume of Fe^{3+} increased to 700 μL, which displays a prominent quenching effect with an efficiency of 100%. Meanwhile, in Fig. 7b, when the volume of Fe^{3+} increased to 1000 μL, the fluorescence emission of activated compound **2** is quenched completely, this quenching effect can be rationalized by the Stern–Volmer equation: $I_0/I = 1 + K_{sv} \times [M]$, where the values I_0 and I are the luminescence intensity of the activated compound **1** or **2** without and with addition of Fe^{3+} solution, respectively, K_{sv} is the quenching constant, [M] is the Fe^{3+} concentration. On the basis of the experimental data in Fig. 7a and b, the linear correlation coefficient (R^2) in the K_{sv} curves of activated **1a** and **2b** are 0.991, 0.995 respectively, which suggests that the quenching effect of Fe^{3+} on the luminescence of activated **1a** and **2b** fit the Stern–Volmer mode well. The K_{sv} value is
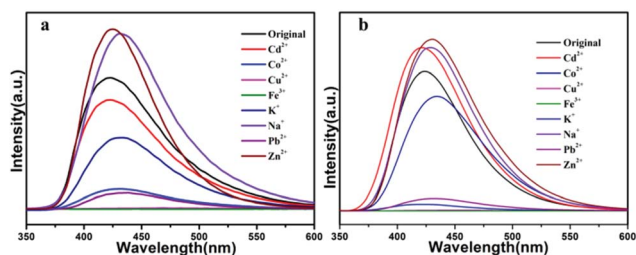

Fig. 6 (a) Fluorescent spectral of compound **1a** in different metal ions (10^{-2} M); (b) fluorescent spectral of compound **2b** in different metal ions (10^{-2} M).
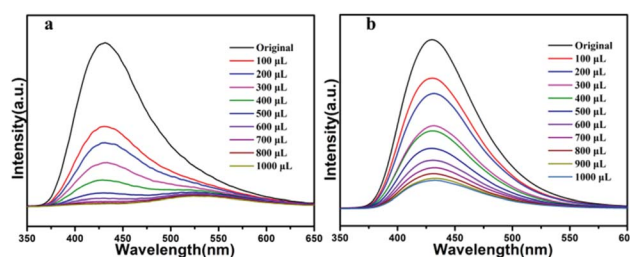

Fig. 7 (a) Fluorescent spectral of compound **1a** dispersed in DMF upon progressive addition of Fe^{3+} solution (10^{-3} M), and the quenching of the original emission and the appearance of a new peak for compound **1**; (b) fluorescent spectral of compound **2b** dispersed in DMF upon progressive addition of Fe^{3+} solution (10^{-3} M).
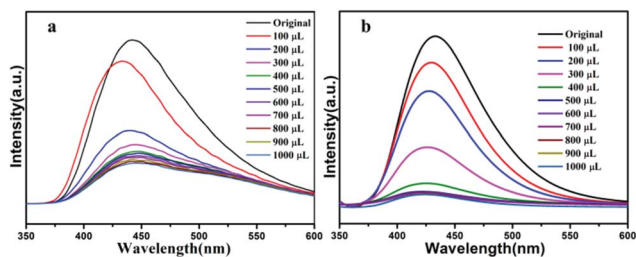
Fig. 8 (a) Fluorescent spectral of compound **1a** dispersed in DMF upon progressive addition of Cu^{2+} solution (10^{-3} M); (b) fluorescent spectral of compound **2b** dispersed in DMF upon progressive addition of Cu^{2+} solution (10^{-3} M).

Fig. 10 (a) Fluorescent spectral of compound **1a** dispersed in DMF upon progressive addition of 10^{-3} M TNP solution; (b) fluorescent spectral of compound **2b** dispersed in DMF upon progressive addition of 10^{-3} M TNP solution.

calculated as 15.5×10^4 M^{-1} and 1.96×10^4 M^{-1} (Fig. S4 and S6†), which reveals a strong quenching effect on the luminescence of the compounds.

With the addition of Cu^{2+} ions, the fluorescence intensity of activated **1** and **2** decrease gradually (Fig. 8a and b). When the concentration of Cu^{2+} ions reaches 1000 μL for activated **1**, the quenching efficiency is 74.2%, and for **2**, when the concentration of Cu^{2+} ions reaches 1000 μL the quenching efficiency is 92.6%, which from S–V curve, the linear correlation coefficient in the K_{sv} curves of activated compound **1** and **2** are 0.9612, 0.964 respectively, the value of K_{sv} is calculated as 1.339×10^4 M^{-1} and 5.64×10^4 M^{-1} (Fig. S5 and S7†), as far as we know, the K_{sv} value is larger than other reported sensors, that is to say, activated **1a** and **2b** can not only detect of Cu^{2+} ions, but also show high sensitivity.[55–57]

Fortunately, the luminescence intensity of activated **1a** and **2b** were easily recovered centrifuging the suspensions after sensing Fe^{3+} or Cu^{2+} ions, and washing more than three times using DMF solvent. Significantly, the samples can be regenerated, the framework retained its structural integrity, and reused for five cycles and the quenching efficiency of the five cycles maintain high values (Fig. S12a, b, S13a and b†). PXRD pattern of the original is completely consistent with the recovered samples with five times of quenching and recovery (Fig. S10a, b, S11a and b†). The results indicate that activated **1a** and **2b** can act as promising chemical sensors for Fe^{3+} and Cu^{2+} ions. The mechanism of luminescence quenching caused by Fe^{3+} and Cu^{2+} might result from interactions between the cations and the framework or central metals.

The nitro aromatic compounds (NACs) are important chemical reactants and are extensively applied in chemical industry, which can cause explosions and environmental damage. Therefore, it is important for fast and effective detection of NACs. As shown from Fig. 9a, the 4-NT, 2-NT, NB have weak quenching efficiency, and 2,6-DNT has weak enhanced luminescent intensities for compound **1**, and 2,6-DNT, and 4-NT, 2-NT, NB, 2,6-DNT have different quenching efficiency for compound **2** in Fig. 9b, meanwhile, preliminary studies show TNP have good quenching efficiency compared with other NACs for both **1** and **2**. For further study the luminescent quenching efficiency of TNP, the fluorescence sensing experiments were carried out by gradual addition of 10^{-3} M solutions of TNP. As shown in Fig. 10a and b, the emission band of compound **1a** and **2b** both undergoes a bathochromic shift ($\Delta\lambda = 50$ nm), which can be ascribed to the energy transfer between electron-rich compound **1** or **2** and electron-deficient TNP.[58,59] the quenching efficiency is 100% at 425 nm when TNP addition reached to 1000 μL for **1** and **2**. To further understand the luminescent quenching degree, the quenching curves were quantitatively studied by the Stern–Volmer equation: $I_0/I = 1 + K_{sv} \times [M]$, the S–V plots exist good linear relationship between the luminescence intensities and the concentration of TNP, and linear correlation coefficient of compound **1** and **2** are up to 0.975, 0.977, according to the S–V equation, the K_{sv} values are up to 2.46×10^4 M^{-1} and 11.76×10^4 M^{-1} for TNP (Fig. S8 and S9†), in addition, in order to study whether the complex can be used as stability material, the dispersed solution was centrifuged after recycled use more than three times. As shown in Fig. S12c and S13c,† compound **1** and **2** can be restored and recycle at least five times. At the same time, the PXRD pattern we tested show good performance compared with the original materials compound **1a** and **2b** (Fig. S10c and S11c†).

Conclusions

Two new 3D supramolecular structures $[Cd_3(L)_2(2,2\text{-bipy})_2(DMF)_3(CH_3CH_2OH)_2(H_2O)$ (**1**) and $[Zn_3(L)_2(2,2\text{-bipy})_2](DMF)_3(H_2O)$ (**2**) based on a fluorescent ligand **H₃L** have been assembled and completely characterized, compound **1** displays a bi-nodal (2,3,6)-coordinated net with $\{8^3\}_2\{8^6 \cdot 12^6 \cdot 16^3\}\{8\}_6$ topology, compound **2** shows a (3,6)-connected 2-nodal net of
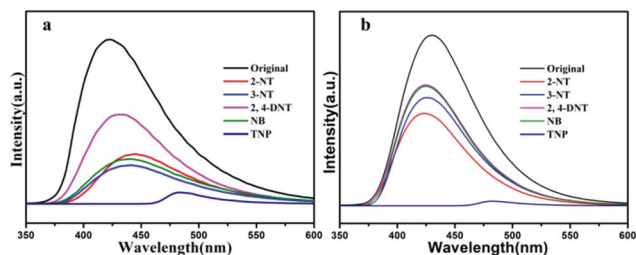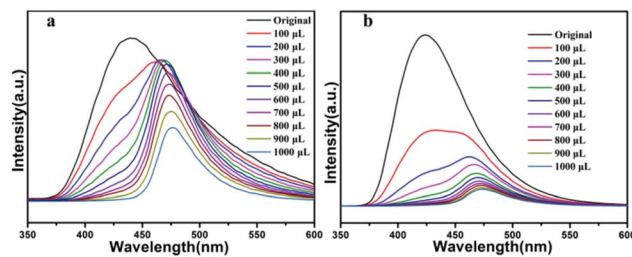

Fig. 9 (a) The fluorescent spectral of **1a** dispersed in 10^{-2} M different DMF solutions of NACs; (b) the fluorescence spectral of **2b** dispersed in 10^{-2} M different DMF solutions of NACs.

kgd topological type. The luminescent properties of the two compounds are measured and investigated in detail, the sensing ability of the two compounds toward metal ions and NACs is studied, revealing their high detection ability to sense Fe^{3+}/Cu^{2+} or TNP *via* luminescence quenching. Hence, the present study demonstrates that the two compounds have the potential applications as dual functional fluorescent sensors for metal ions and NACs.

Conflicts of interest

There are no conflicts to declare.

Acknowledgements

Notes and references

1 X. Fang, B. Y. Zong and S. Mao, *Nano-Micro Lett.*, 2018, 1–19.
2 S. A. Diamantis, A. Margariti, A. Pournara, G. S. Papaefstathiou, M. J. Manos and T. Lazarides, *Inorg. Chem. Front.*, 2018, 5, 1493–1511.
3 Z. C. Hu, B. J. Deibert and J. Li, *Chem. Soc. Rev.*, 2014, 43, 5815–5840.
4 B. Y. Li, Y. M. Zhang, D. X. Ma, Z. Shi and S. Q. Ma, *Nat. Commun.*, 2014, 5(5537), 1–7.
5 W. F. Xu, H. H. Chen, Z. Q. Xia, C. T. Ren, J. Han, W. J. Sun, Q. Wei, G. Xie and S. P. Chen, *Inorg. Chem.*, 2019, 58, 8198–8207.
6 C. Liu, X. J. Bo and L. P. Guo, *Sens. Actuators, B*, 2019, 297, 126741.
7 X. D. Yu, G. B. Guo, P. Peng, F. J. Shen, Y. J. Li, L. J. Geng and T. Wang, *Appl. Surf. Sci.*, 2019, 487, 473–479.
8 L. N. Wang, Y. H. Zhang, S. Jiang and Z. Z. Liu, *CrystEngComm*, 2019, 21, 4557–4567.
9 J. H. Wei, J. W. Yi, M. L. Han, B. Li, S. Liu, Y. P. Wu, L. F. Ma and D. S. Li, *Chem.–Asian J.*, 2019, 14, 3694–3701.
10 W. Wang, J. Yang, R. M. Wang, L. L. Zhang, J. F. Yu and D. F. Sun, *Cryst. Growth Des.*, 2015, 15, 2589–2592.
11 S. N. Zhao, X. Z. Song, M. Zhu, X. Meng, L. L. Wu, S. Y. Song, C. Wang and H. J. Zhang, *RSC Adv.*, 2015, 5, 93–98.
12 E. L. Zhou, P. Huang, C. Qin, K. Z. Shao and Z. M. Su, *J. Mater. Chem. A*, 2015, 3, 7224–7228.
13 K. M. Wollin and H. H. Dieter, *Arch. Environ. Contam. Toxicol.*, 2005, 49, 18–26.
14 K. W. Hofmann, H. J. Knackmuss and G. Heiss, *Arch. Environ. Contam. Toxicol.*, 2004, 70, 2854–2860.
15 C. H. Chen, X. S. Wang, L. Li, Y. B. Huang and R. Cao, *Dalton Trans.*, 2018, 47, 3452–3458.
16 F. L. Hu, Y. X. Shi, H. H. Chen and J. P. Lang, *Dalton Trans.*, 2015, 44, 18795–18803.
17 B. B. Andrea, A. M. Costero, G. Salvador, P. Margarita, J. Soto, M. M. Ramon and F. Sancenonz, *Chem. Commun.*, 2012, 48, 3000–3002.
18 J. L. Bricks, A. Kovalchuk, C. Trieflinger, N. Marianne, B. Michael, A. I. Tolmachev, J. Daub and K. Rurack, *J. Am. Chem. Soc.*, 2005, 127, 13522–13529.
19 H. Li, Y. J. Li, Z. Zhang, X. L. Pang and X. D. Yu, *Mater. Des.*, 2019, 172, 107712.
20 Y. Y. Liang, L. J. Luo, Y. Li, B. K. Ling, B. W. Chen, X. W. Wang and T. G. Luan, *Eur. J. Inorg. Chem.*, 2019, 206–211.
21 Y. L. Wu, G. P. Yang, Y. Q. Zhao, W. P. Wu, B. Liu and Y. Y. Wang, *Dalton Trans.*, 2015, 44, 3271–3277.
22 L. M. Gaetke and C. K. Chow, *Toxicology*, 2003, 189, 147–163.
23 M. Petrovic, M. Farréa, M. L. Aldaa, S. Perez, C. Postigo, K. Marianne, J. Radjenovic, G. Merixell and D. Barcelo, *J. Chromatogr. A*, 2010, 1217, 4004–4017.
24 Z. O. Tesfaldet, J. F. Staden and R. I. Stefan, *Talanta*, 2004, 64, 1189–1195.
25 K. Håkansson, R. V. Coorey, R. A. Zubarev and V. L. Talrose, *J. Mass Spectrom.*, 2000, 35, 337–346.
26 A. C. Liu, D. C. Chen, C. C. Lin, H. H. Chou and C. H. Chen, *Anal. Chem.*, 1999, 71, 1549–1552.
27 V. A. Elrod, K. S. Johnson and K. H. Coale, *Anal. Chem.*, 1991, 63, 893–898.
28 M. Saleem and K. H. Lee, *RSC Adv.*, 2015, 5, 72150–72287.
29 P. Kovacic and R. Somanathan, *J. Appl. Toxicol.*, 2014, 34, 810–824.
30 M. Formica, V. Fusi, L. Giorgi and M. Micheloni, *Coord. Chem. Rev.*, 2012, 256, 170–192.
31 G. M. Espallargas and E. Coronado, *Chem. Soc. Rev.*, 2018, 47, 533–557.
32 H. X. Liang, X. L. Jiao, C. Li and D. R. Chen, *J. Mater. Chem. A*, 2018, 6, 334–341.
33 P. L. Wang, L. H. Xie, E. A. Joseph and J. R. Li, *Chem. Rev.*, 2019, 119, 10638–10690.
34 Z. X. Kang, L. L. Fan and D. F. Sun, *J. Mater. Chem. A*, 2017, 5, 10073–10091.
35 A. H. Chughtai, N. Ahmad, H. A. Younus, A. Laypkov and F. Verpoort, *Chem. Rev.*, 2015, 44, 6804–6849.
36 J. W. Liu, L. F. Chen, H. Cui, J. Y. Zhang, L. Zhang and C. Y. Su, *Chem. Soc. Rev.*, 2014, 43, 6011–6061.
37 R. B. Getman, Y. S. Bae, C. E. Wilmer and R. Q. Snurr, *Chem. Rev.*, 2012, 112, 703–723.
38 J. R. Li, J. Sculley and H. C. Zhou, *Chem. Rev.*, 2012, 112, 869–932.
39 Y. J. Cui, Y. F. Yue, G. D. Qian and B. L. Chen, *Chem. Rev.*, 2012, 112, 1126–1162.
40 A. Corma, H. García and F. X. Liabrés i Xamena, *Chem. Rev.*, 2010, 110, 4606–4655.

41 A. J. Lan, K. H. Li, H. H. Wu, D. H. Olson, T. G. Emge, W. Ki, M. C. Hong and J. Li, *Angew. Chem., Int. Ed.*, 2009, **48**, 2334–2338.

42 D. X. Ma, B. Y. Li, X. J. Zhou, Q. Zhou, K. Liu, G. Zeng, G. H. Li, Z. Shi and S. H. Feng, *Chem. Commun.*, 2013, **49**, 8964–8966.

43 D. Tian, Y. Li, R. Y. Chen, Z. Chang, G. Y. Wang and X. H. Bu, *J. Mater. Chem. A*, 2014, **2**, 1465–1470.

44 S. S. Nagarkar, B. Joarder, A. K. Chaudhari, S. Mukherjee and S. K. Ghosh, *Angew. Chem., Int. Ed.*, 2013, **52**, 2881–2885.

45 J. Wang, J. Wu, L. Lu, H. J. Xu, M. Trivedi, A. Kumar, J. Q. Liu and M. B. Zheng, *Front. Chem.*, 2019, **7**, DOI: 10.3389/fchem.2019.00244.

46 E. L. Zhou, C. Qin, D. Tian, X. L. Wang, B. X. Yang, L. Huang, K. Z. Shao and Z. M. Su, *J. Mater. Chem. C*, 2018, **6**, 7874–7879.

47 J. S. Hu, T. T. Cheng, S. J. Dong, C. H. Zhou, X. H. Huang and L. Zhang, *Microporous Mesoporous Mater.*, 2018, **272**, 177–183.

48 Z. Z. Shi, Z. R. Pan, H. L. Jia, S. G. Chen, L. Qin and H. G. Zheng, *Cryst. Growth Des.*, 2016, **16**, 2747–2755.

49 L. Hu, X. J. Hong, X. M. Lin, J. Lin, Q. X. Cheng and B. Lokesh, *Cryst. Growth Des.*, 2018, **18**, 7088–7093.

50 X. J. Zhou, B. Y. Li, G. H. Li, Q. Zhou, Z. Shi and S. H. Feng, *CrystEngComm*, 2012, **14**, 4664–4669.

51 Z. H. Yan, W. Wang, L. L. Zhang, X. W. Zhang, L. Wang and D. F. Sun, *RSC Adv.*, 2015, **5**, 16190–16198.

52 J. G. Lin, S. Q. Zang, Z. F. Tian, Y. Z. Li, Y. Y. Xu, H. Z. Zhu and Q. J. Meng, *CrystEngComm*, 2007, **9**, 915–921.

53 Y. P. Li, X. H. Zhu, S. N. Li, Y. C. Jiang, M. C. Hu and Q. G. Zhai, *ACS Appl. Mater. Interfaces*, 2019, **11**, 11338–11348.

54 J. C. Jin, L. Y. Pang, G. P. Yang, L. Hou and Y. Y. Wang, *Dalton Trans.*, 2015, **44**, 17222–17228.

55 J. Y. Liang, G. P. Li, R. C. Gao, N. N. Bai, W. Q. Tong, L. Hou and Y. Y. Wang, *Cryst. Growth Des.*, 2017, **17**, 6733–6740.

56 J. M. Zhou, W. Shi, H. M. Li, H. Li and P. Cheng, *J. Phys. Chem. C*, 2014, **118**, 416–426.

57 Y. Q. Xiao, Y. G. Cui, Q. Zheng, S. C. Xiang, G. D. Qian and B. L. Chen, *Chem. Commun.*, 2010, **46**, 5503–5505.

58 A. Gogia and S. K. Mandal, *Dalton Trans.*, 2019, **48**, 2388–2398.

59 S. Mukherjee, A. V. Desai, B. Manna, A. I. Inamdar and S. K. Ghosh, *Cryst. Growth Des.*, 2015, **15**, 4627–4634.